Electrochemical Materials and Technologies

ARTICLE

Electrochemical Materials and Technologies

eISSN: 2949-0561

Cite this: Electrochem. Mater. Technol. 3 (2024) 20243046

$(Y_{0.82}La_{0.18})_3Fe_5O_{12-x}$: structure and transport properties

Sergey Shkerin [a]*, Anna Tolkacheva [b], Sergey Naumov [c]*, Olga Gyrdasova [d], Anton Stepanov [c]

Received: 7 November 2024
Accepted: 29 November 2024
Published online: 16 December 2024

DOI: 10.15826/elmattech.2024.3.046

The nonstoichiometry in well-known rare-earth metal ferrite garnets is discussed in the concept of a mayenite analogue. Crystals are grown by floating zone method in different atmospheres. The content of oxygen during the growth process determines its crystal structure: only in an oxygen atmosphere (7 atm) is it possible to obtain a single-phase crystal. The phase decomposes with precipitation of iron oxide when the content of oxygen is lower. The decomposition is also induced by the replacement of Y with a large cation La in $Y_3Fe_5O_{12}$. The fibers of the perovskite phase form along the crystal growth direction. The high mobility of anions and electron conductivity are shown by the method of isotopic equilibration with the gas phase on single-crystal garnet composites.

keywords: rare-earth metal ferrite garnet, anions conductivity, electron conductivity, single crystal

1. Introduction

Cubic structure materials demonstrate high oxygen-ion conductivity due to the high concentration of oxygen vacancies and their mobility. Among these materials, fluorites based on zirconium, hafnium, thorium, cerium, and uranium oxides are studied in the most detail. The first publication on doped zirconia was published in 1898 [1]. Solid electrolytes based on doped lanthanum gallate with the perovskite structure have been widely discussed since 1994 [2, 3].

Among all garnets, rare-earth metal (*REM*) ferrites of general composition $M_3Fe_2Fe_3O_{12}$ attract increasing attention due to a number of unique features, such as thermochromism [4] and anomalies in magnetic properties [5–11].

a: The Institute of High-Temperature Electrochemistry UB RAS, Ekaterinburg 620066, Russia
b: Ural Federal University, Ekaterinburg 620002, Russia
c: M.N. Mikheev Institute of Metal Physics UB RAS, Ekaterinburg 620137, Russia
d: Institute of Solid-State Chemistry UB RAS, Ekaterinburg 620137, Russia

* Corresponding authors: S.V. Naumov (naumov@imp.uran.ru), S.N. Shkerin (shkerin@mail.ru)

Studies on solid solutions of yttrium iron garnets [12–18], like many others, considered the ideal structure of garnet (not containing vacancies in the cation sublattice). However, the garnet structure contains intrinsic cation vacancies. This is most clearly manifested for the position of cations surrounded by 8 oxygen anions, where the proportion of vacancies can reach 1/6 [19]. The crystal chemistry appoints to a garnet structure to contain three types of cations, differing in coordination number. These three types of positions are forced to coexist in the same structure, which imposes strict restrictions on the ratios of the sizes of the cations occupying them.

At the same time, the irreproducibility of the listed properties is noted [20] and its reason could be the variable oxygen stoichiometry. Non-stoichiometric oxygen conductive garnets have been represented quite recently [21]. The most discussed among them is calcium aluminate – mayenite.

The optimal way to estimate the oxygen vacancy concentration in the compound is to study its oxygen-ion conductivity. According to a rough estimate, it is about 3 % [22]. This issue was later explored in more detail

[23–26]. It is generally accepted that the oxygen-ion conductivity of garnets should be lower than that of perovskites [25] and confirmed by direct measurements of the oxygen anions self-diffusion [27, 28] for garnets with low oxygen nonstoichiometry. However, a particular substitution of yttrium cations by a divalent cation significantly increases the oxygen-ion conductivity [25]. The maximum of dopant succeeds in 1/6 yttrium positions [25].

The possibility of substitution up to 1/6 cations in the A position in the garnet lattice, even for vacancies, was considered in detail earlier [21]. Is it possible to implement this in practice in order to increase the oxygen-ion conductivity?

The main problem in the design of such compounds is the stability of garnet with a high concentration of defects. The formation of a surface layer with a low defect concentration and, as a consequence, low transport properties is described for calcium aluminate [21, 29, 30].

The unexpected effect of stabilization in the highly defective structure is described by Bhosale [31]. The large cation La^{3+} was introduced into the lattice of yttrium iron garnet which leads to the formation of $LaFeO_3$ perovskite clusters and regions with a garnet structure, where the non-stoichiometry is similar to described one in mayenite [21]. We avoided using additional cations of variable valency so that the entire change in oxygen activity was determined by the ratio of the Fe^{2+}/Fe^{3+} concentrations.

The presence of a positive effect on conductivity without discussion its nature is also described by Yousa [32]. The reported total conductivity shows a tremendous variation in ionic conductivity from 10^{-11} to 10^{-2} S · cm^{-1} at 450 °C [31].

This study is aimed to elucidate the synthesis procedure, the electrical properties of yttrium ferrite doped with lanthanum using single-crystal or dense ceramics, and oxygen exchange process to verify the nature of electrical conductivity up to 800 °C which is close to using one in SOFC technology.

2. Experimental

2.1. Single crystal fabrication

The previous investigation showed that synthesis by thermal decomposition of complex formate $(Y_{0.82}La_{0.18})_3Fe_5[HCOO]_{24} \cdot nH_2O$ gives the maximum of product yield [33].

$Y(NO_3)_3$, $La(NO_3)_3$ were obtained from the corresponding oxides by the action of concentrated nitric acid. To a stoichiometric mixture of the obtained nitrates and $Fe(NO_3)_2 \cdot 6H_2O$, concentrated formic acid (analytical grade) was gradually added until the emission of nitrogen oxides ceased [34]. The reaction product was mixed formate $(Y_{0.82}La_{0.18})_3Fe_5[HCOO]_{24} \cdot nH_2O$, which was annealed at 600 °C to decompose and remove the oxidation products of the formate group carbon. Ceramics were prepared in the form of a 5 x 5 x 50 mm^3 bar at 1300 °C for 12 hours.

A single crystal was grown by the floating zone method in URN-2-3P 5 kW plant (Moscow Power Engineering Institute) at an oxygen pressure of 7 atm using ceramics as a half-way product.

The precursor and crystal morphology were studied using a JEOL JSM-6390LA scanning electron microscope (SEM) in BSE imaging mode with an acceleration voltage of 30 kV and resolving power of 3.0 nm.

X-ray phase analysis was carried out on an STADI-P diffractometer (STOE) operating with CrK_{a1} radiation. The patterns were compared with those in PDF-2 (ICDD Release 2016).

2.2. Conductivity measurements

The kinetics of interaction of oxygen from the gas phase with ferrogarnet was investigated by the method of oxygen isotope exchange under static isothermal conditions. Single crystal samples $(Y_{0.82}La_{0.18})_3Fe_5O_{12}$ were formed as a thin slab and cut along the direction of crystal growth. The samples thickness did not exceed 1 mm. Its attestation by X-ray diffraction proved single phase and garnet crystal structure (see Figure S2 in Supplementary).

The samples surface was polished with diamond paste, after which they were placed in a quartz reactor and annealed at 900 °C in oxygen to remove excess of paste and organic solvents. Heating the sample under the experimental conditions was carried out in natural isotopic composition for at least a day to establish equilibrium. The next step was to change the atmosphere above the sample. An isotopic oxygen composition was added to the circuit connected to the reactor; the pressure in the circuit was equal to the pressure in the reactor. The beginning of the experiment was considered to be the opening of a valve between the reactor and the circuit, that is, the moment the oxygen isotopes began to mix. Changes in kinetic dependencies of G_{32}, G_{34}, and G_{36} on concentration of oxygen isotopes associated with $^{16}O_2$, $^{16}O^{18}O$, $^{18}O_2$, and the background line over time were recorded using a quadrupole mass spectrometer (see Figure S3 in Supplementary). The end of the experiment is to establish an equilibrium of the isotopic composition in the gas mixture.

The model by Ezin et al. [35] on the basis of the Kliers K. et al. solution [36] is used to calculate the values of r_H (atom/(cm^2 · s)) and D (cm^2/s).

This model is the result of two solutions for the simultaneous-equation system with boundary and initial conditions:

$$\begin{cases} \frac{N}{S}\dot{a} = r_H(\alpha_S - \alpha) \\ \frac{N}{S}\dot{y} = -ry + 2r_2(\alpha_s - \alpha)^2, \\ \dot{a} = D\nabla^2\alpha \\ r = r_0 + r_1 + r_2 \end{cases} \quad (1)$$

where S is a surface area of the sample; N is the amount of oxygen in a gas phase; α (alpha) is the oxygen isotope ^{18}O fraction; α_s is the ^{18}O-fraction at the oxide surface, r_H is the interfacial exchange rate; y is a difference between the concentration of $^{18}O^{16}O$ molecules at time τ and the equilibrium concentration of $^{18}O^{16}O$ molecules; D is the diffusion coefficient of tracer oxygen and r_0, r_1 and r_2 are the rates of the three exchange types. Indexes 0, 1 and 2 show the amount of oxygen from the surface, which interacts in one exchange type, and r is a sum of the rates for the three exchange types. The solution of equations system gives both α and y time dependencies connected with the concentration of molecular oxygen in the gas phase with a different isotope composition:

$$C_{32}(t) = (1-\alpha)^2 + {}^{y}/_{2}, \quad (2)$$

$$C_{34}(t) = 2\alpha(1-\alpha) - y, \quad (3)$$

$$C_{36}(t) = \alpha^2 + {}^{y}/_{2}. \quad (4)$$

$C_{32} = f(t)$, $C_{34} = f(t)$ and $C_{36} = f(t)$ minimization allows calculating r_H, r, r_2 and D. The sum of squared residuals is used as a minimizing function:

$$\sigma = \sum(C_{32}^{exp} - C_{32}^{theor})^2 + \sum C_{34}^{exp} - C_{34}^{theor})^2 + \\ + \sum(C_{36}^{exp} - C_{36}^{theor})^2. \quad (5)$$

The error isoline procedure (see Figure S3 in Supplementary) was used to assess the accuracy of the determination of exchange and oxygen diffusion coefficients. This model was previously described in detail [37] for the isotopic exchange where the experimental data are the distribution of the label over the sample.

The kinetic dependences of C_{32}, C_{34}, and C_{36} on concentration of oxygen isotopes were used to calculate the exchange rates of three types of r_0, r_1 and r_2 according to the Ezin's model.

The values of three types of oxygen exchange were used to calculate the elementary stages of oxygen exchange: dissociative adsorption and oxygen incorporation, using the approach of Ananyev et al. [38].

3. Result and discussion

3.1. Crystal chemistry

Precursors for synthesis were qualified as unstructured polycrystals of about 80 nm (see Figure S4 in Supplementary), according to the SEM.

X-ray data established in Table 1 and Figure 1 illustrate the phases presented in precursors after calcination at 600 °C in air (Figure 1a), ceramics annealed at 1300 °C (Figure 1b) and powders obtained by grinding $(Y_{0.82}La_{0.18})_3Fe_5O_{12}$ crystals (Figure 1c).

The powders shown in Figure 1 contain 3 phases: perovskite of estimated composition La(Y)FeO_3, Fe_2O_3 and yttrium iron garnet $(YLa)_3Fe_5O_{12}$.

The melting point of ceramics is sensitive to oxygen pressure. The results presented in Table 1 correspond to an oxygen pressure of 7 atm, however, in argon (4 atm) the appearance of FeO is observed and ceramics melting point drops significantly. X-ray diffraction of such a product shows the following weight fractions:

- perovskite $YFeO_3$ ~ 74 mol. %
- FeO ~ 12 %,
- Y_2O_3 ~ 6 %,
- garnet ~ 5 %,
- Fe_3O_4 ~ 3 %.

This result is expected according to the values of the ionic radii (Table 2). As mentioned above, the garnet structure contains three types of cation positions, with the following coordination numbers: $^{(VIII)}A_3{}^{(VI)}B_2{}^{(IV)}C_3O_{12}$.

The radii of cations in these positions correspond to size relations of stability in structure. The smallest cation is located in the tetrahedral position (*C*). Cationic vacancies are not allowed for it. That is why the tetrahedral sites are predominantly occupied by trivalent iron cations.

Table 1 – Phase composition and lattice parameters of $(Y_{0.82}La_{0.18})_3Fe_5O_{12}$.

Sample	Weight fractions for pattern, %			*a*, (Å)
	Fe_2O_3	La(Y)FeO_3	$(YLa)_3Fe_5O_{12}$	
precursor	38.4	55.6	6	–
ceramics	–	–	100	12.437(3)
crystal powder	5.6	7.6	86.6	12.432(5)

Table 2 – Ionic radii of cations depending on the environment symmetry.

Coordination number	Ion radii, Å			
	Fe^{3+}	Fe^{2+}	La^{3+}	Y^{3+}
4	0.49	0.63	–	–
6	0.55	0.61	1.03	0.90
8	0.79	0.92	1.16	1.02

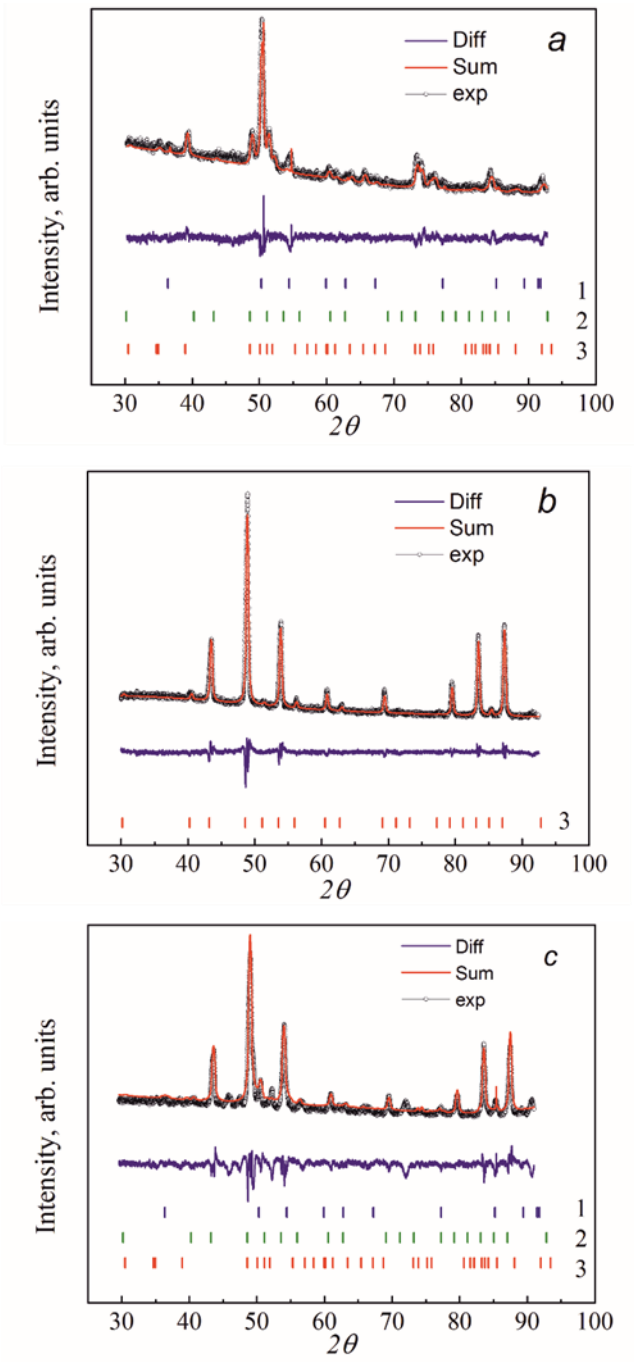

Figure 1 X-ray patterns of $(Y_{0.82}La_{0.18})_3Fe_5O_{12}$: (a) – precursors prepared via thermolysis; (b) – product after sintering at 1300 °C; (c) – powdered composite. The position of the Bragg peaks is shown by dashes: 1 – Fe_2O_3, 2 – La(Y)FeO_3, 3 – $(YLa)_3Fe_5O_{12}$ (exp – experiment, sum – calculation, diff – difference between experiment and calculation).

Therefore, Fe^{2+} cations occupy *A* position (*CN* = 8) and *B* position (*CN* = 6). Moreover, vacancies appear on these sites; nevertheless, the concentration of cationic vacancies on *B* position is low. The concentration of cationic vacancies in *A* position rises up to 1/6.

The ratio Fe^{2+}/Fe^{3+} depends on the oxygen partial pressure: $V_O + 2Fe^{2+} + 1/2\,O_2(g) = O^{\times} + 2Fe^{3+}$.

The same equation in short form: $Fe^{2+} + 1/4\,O_2(g) = Fe^{3+}$.

Thus, a certain critical oxygen atmosphere makes Fe^{3+} cations occupy all sites in the *C* sublattice. This pressure is higher in fact, since Fe^{3+} cations also occupy positions *B* and *A*. If the oxygen partial pressure is below the critical value, then the $YFeO_3$ or $LaFeO_3$ perovskite appears simultaneously with the garnet structure, since the diversity in the size and charge of the iron cation is less critical for perovskite. Note that the perovskite with maximum defects in the structure is brownmelerite ($ABO_{2.5}$). As follows from Table 1, $pO_2 = 7$ atm is sufficient oxygen activity to produce a single-phase $(Y_{0.82}La_{0.18})_3Fe_5O_{12}$ garnet.

As was mentioned above, a high concentration of vacancies in the A site in the garnet structure is possible. Their appearance also produces a significant amount of anion vacancies, associates of cationic and anionic defects, which creates a number of unique properties [21]. However, such materials have low stability. A small displacement between positions, accompanied by oxygen exchange between the crystal and gas phase, turns a highly nonstoichiometric garnet into ordinary garnet. An example of such transformation was observed earlier [29, 30], where a surface layer with low transport properties on mayenite (calcium aluminate) is shown.

An original method for designing the structure of mayenite-like highly nonstoichiometric garnet from yttrium iron garnet was discussed by D.R. Bhosale [31]. As was mentioned above, there are strict requirements for the cations size ratio in different sublattices of garnet. La^{3+} is too large and the partial substitution of Y^{3+} by La^{3+} forms a solid solution with internal mechanical stresses, in which clusters with a perovskite structure based on lanthanum ferrite appear at room temperature in matrix mayenite-like yttrium iron garnet. The anomalous anion transport was predicted on the base of its high-temperature neutron diffraction data [31]. The present work is the first experimental study of this concept.

The crystals grown by the floating zone method are single phase $(Y_{0.82}La_{0.18})_3Fe_5O_{12}$ according to Figure 1b and non-porous microstructure (see Figure S4 in Supplementary).

The crystal growth direction corresponds to the <100> direction of the garnet lattice (Figure 2). However, detailed studies revealed inhomogeneity (see Table 1). Fibers of another composition with submicron cross-section are formed in the direction of crystal growth [30]. The ratio between the concentrations of iron cations and [La + Y] makes it possible to denote this second phase to a perovskite structure.

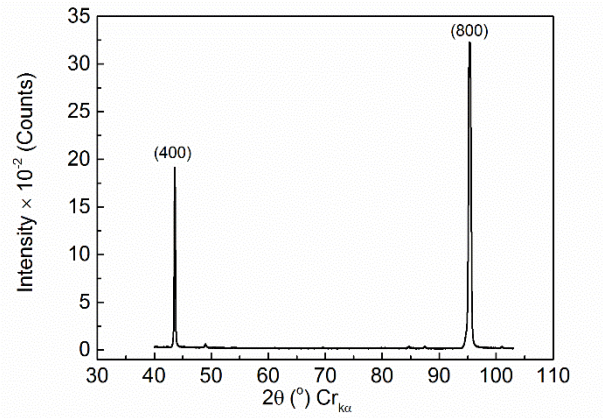

Figure 2 X-ray pattern fragments of plane perpendicular to the direction of crystal growth.

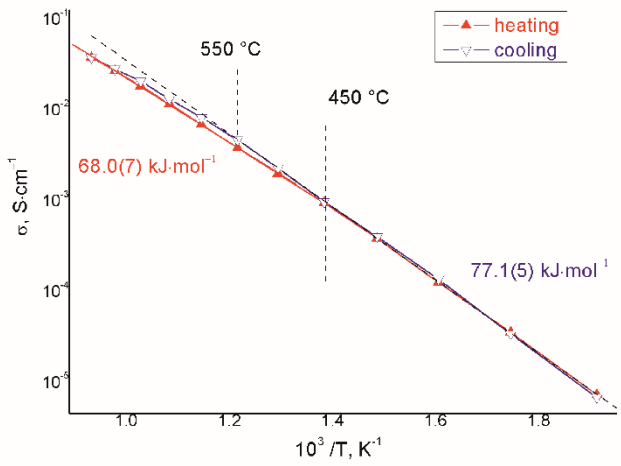

Figure 3 Temperature dependence of total electrical conductivity measured by impedance spectroscopy in a symmetrical cell with Pt electrodes.

During setting the research task, we expected the formation of domains with the $LaFeO_3$ perovskite structure uniformly distributed in the volume. The reason for this effect is the mismatch between cation radii La^{3+} and Y^{3+} for the $Y_3Fe_5O_{12}$ garnet lattice. The appearance of fibers that are evenly spaced apart from each other instead of clusters indicates a significant nonadiabaticity of the crystal growth conditions during experiments.

The garnet structure regions around perovskite inclusions are depleted in yttrium cation and correspond to nonstoichiometric garnet, similar to the mayenite structure. This type of structure demonstrates increased transport properties.

3.2. Electrical conductivity

Conductivity was previously studied when heated (Figure 3). The crystal sample was exposed for 300 hours at 800 °C in air, while its resistance slightly drifted from 39.8 to 38.2 Ohm (Figure 3) before the measurements of the temperature dependence of conductivity when cooling started.

Figure 3 shows a comparison of temperature dependencies obtained during initial heating and during cooling after exposure. A weak hysteresis is visible above 450 °C. The absence of a frequency dependence of electrical conductivity indicates the dominant electronic transport (see Figure S5 in Supplementary), which is in good agreement with the literature data [25]. Note that a slight increase in conductivity upon 50 hours of equilibration time for the composition $Y_{2.5}Ca_{0.5}Fe_5O_{12-\delta}$ was also reported earlier [25].

The measurable electronic conductivity of oxides containing iron cations in charge states two and three is well known. It is determined by electron transfer between Fe^{2+} and Fe^{3+}, as commonly used, by polaron mechanism.

The isolation of oxygen-ion conductivity against the background of high electronic conductivity is a complex problem that can only be solved by the method of isotope exchange, which was done in this study.

The mobile ions can play an important role due to their redistribution throughout the volume when constant current polarization is applied for a long time. This inevitably leads to a change in the composition of the sample in volume.

The degradation of the samples is observed at 800 °C along the precipitation of iron oxide during isotope measurements carried out at low oxygen pressure. A similar process is also observed in electrical conductivity measurements. During the experiments, fibers of the perovskite structure grow to a micron in diameter and are determined by the X-ray diffraction method.

3.3. The oxygen isotope exchange

After XRD attestation of the samples (see Figure S2 in Supplementary), the crystal slab was equilibrated with the oxygen atmosphere. When the sample distinguished a balance before the isotope experiment, an unusual decrease in pressure was observed (see Figure S6 in Supplementary). The reduction in oxygen pressure ranged from 10.20 to 9.52 mbar in 72 h, which is not large compared to the time of a single experiment. On the one hand, such behavior of the system does not fit the model used to results processing. On the other hand, this fact was not taken into account before, as all previously obtained results on oxygen diffusion in $Y_3Fe_5O_{12-\delta}$ were obtained by the method of secondary-ion mass spectroscopy (SIMS) [27, 28]. Such effects are not evidenced by SIMS, even if they occur.

After exposure for 72 h in oxygen of natural composition, the atmosphere was replaced with a chemically identical one enriched with a heavy isotope. The time dependence of the concentration of heavy

oxygen in the gas phase (Figure 4) and the proportions of specific molecules (Figure 5) were used for the calculating of the rate of heterogeneous exchange (Figure 6) and the diffusion coefficient of oxygen (Figure 7).

The assumption about a surface layer makes it to divide the rate of heterogeneous exchange (Figure 6) into components (Figure 8): adsorption (a characteristic of exchange between the gas and the layer) and incorporation (a characteristic of exchange between the layer and the volume).

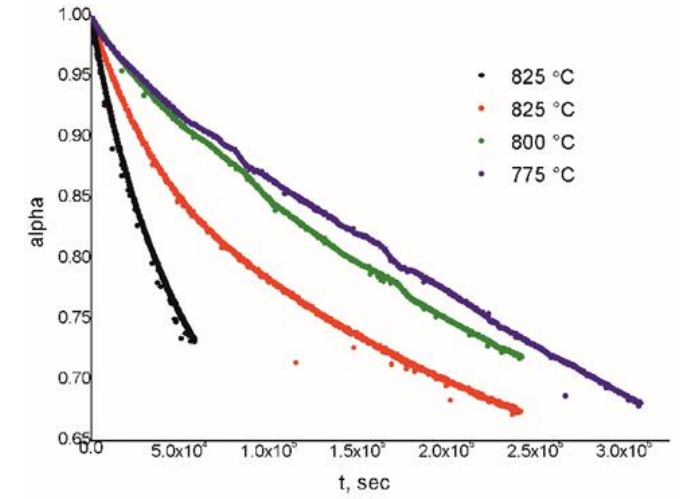

Figure 4 Time dependence of the ^{18}O isotope fraction at 775–825 °C temperature range.

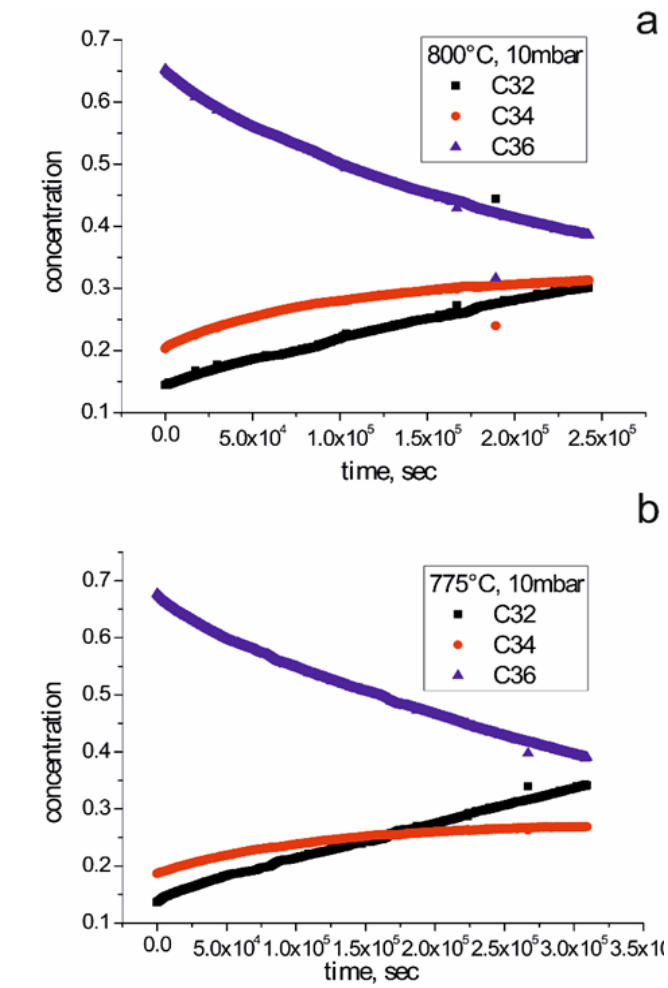

Figure 5 Isobaric time dependencies of the change in molecules proportions with masses 32, 34 and 36 for experiments at (a) – 800 °C (b) – and 775 °C.

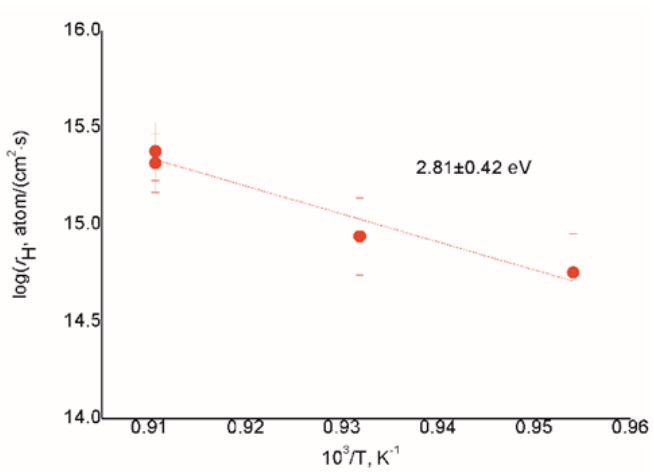

Figure 6 Isobaric (10 mbar) time dependence of heterogeneous oxygen exchange velocity [r_H, atom/(cm^2 · sec)].

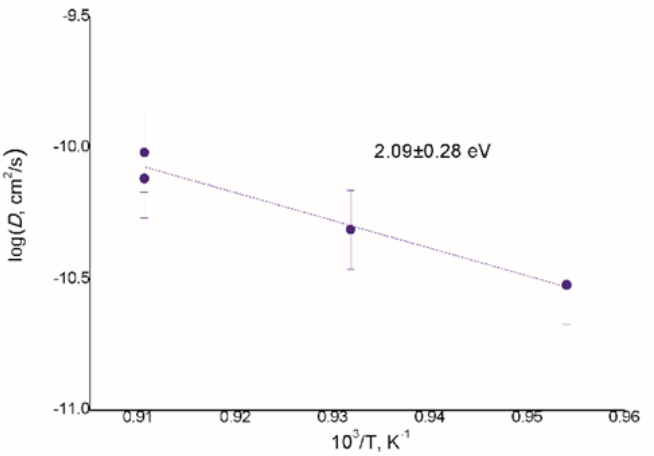

Figure 7 Isobaric (10 mbar) time dependence of diffusion coefficient of oxygen [D, cm^2/sec].

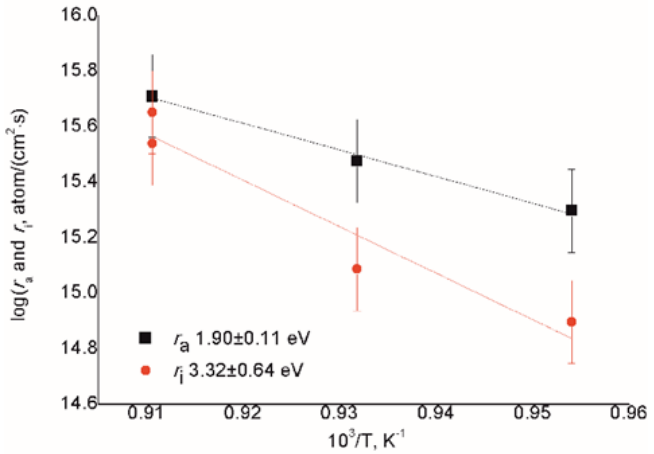

Figure 8 Temperature dependencies of the oxygen adsorption (r_a) and incorporation (r_i) rates.

In order to find out the reasons for the drift of oxygen pressure in the chamber (see Figure S6 in Supplementary), we carried out the X-ray study of the sample after measurements (see Figure S7 in Supplementary). Two garnets with a slight difference between the cell parameter and the presence of FeO (PDF 79-2175) are found. The oxygen utilization is used to occur by this mechanism: $Fe^{2+} + 1/4\,O_2(g) = Fe^{3+}$, due to the electro neutrality requirement. Thus, the appearance of Fe^{2+} evidences the loss of stability in the garnet structure upon exposure to an atmosphere with increased oxygen activity.

Measurement of electrical conductivity (Figure 3) also changed samples. Submicron fibers penetrating the volume along the axis of crystal growth [33], increased in diameter up to several microns (see Figure S8 in Supplementary). From the requirement to balance of cation concentration, estimated using an electron microscope, these fibers correspond to the perovskite structure. Note that the lattice parameter of the garnet has changed – if the initial was 12.432 Å, then after 300 h of exposure at 800 °C it became 12.424 Å. A displacement of large cations from the garnet structure into the perovskite structure in the decomposition process seems to be the most probable reason for this experimental fact. The tendency of a garnet structure to decay with the release of a perovskite structure was already discussed earlier [39]. Figure 9 shows the comparison of our results on diffusion coefficient obtained by isotopic methods with previous ones both on ceramics and single crystals [27, 28].

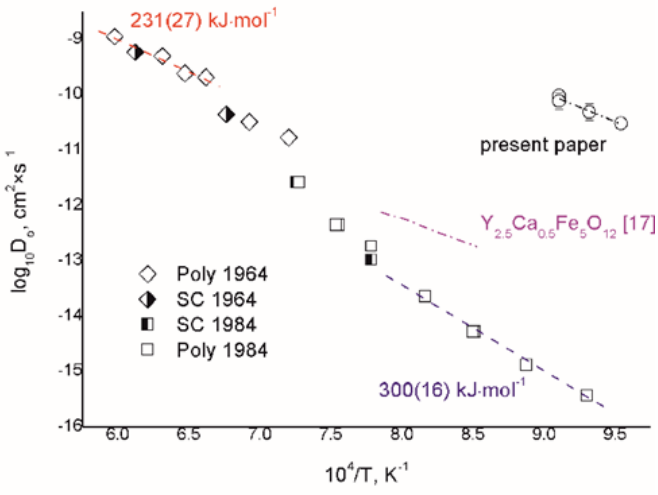

Figure 9 The oxygen diffusion coefficient: comparison of our results (circles) with the literature data for undoped $Y_3Fe_5O_{12-\delta}$ (diamonds [27], squares [28], open symbols for ceramics, otherwise for single crystals). The dotted line shows the estimate for $Y_{2.5}Ca_{0.5}Fe_5O_{12-\delta}$ composition [25].

Undoped $Y_3Fe_5O_{12-\delta}$ demonstrates two segments on the presented curve. The first one near the melting point has a diffusion activation energy slightly higher than 2 eV. The second one below 1020 °C is described by significantly lower oxygen mobility and a diffusion activation energy of about 3 eV. Between these regions, there is a transitional region that seems to be poorly reproducible. The activation energy of oxygen anion transfer in the low-temperature region is characteristic of undoped aluminate and gallate garnets [40, 41]. For a maximum doped (1/6 positions *A*) ferrite with a garnet structure $Y_{2.5}Ca_{0.5}Fe_5O_{12-0.25-\delta}$, the activation energy of anionic conduction is of about 2 eV [25]. Assuming that all oxygen anions take part in the transfer, the data on conductivity [25] using the Nernst-Einstein relation were recalculated into the diffusion coefficient (Figure 9).

The activation energy of the oxygen diffusion coefficient for the studied material is also of about 2 eV (Figure 7), which indicates an oxygen transfer mechanism similar to that implemented in the high-temperature modification of undoped garnet [27] and garnet with 1/6 of the yttrium cations replaced by calcium cations [25]. If the Ca_Y defect [17] creates ½ of the oxygen vacancy, then the $[\_]_Y$ cation vacancy creates 1½. Apparently, this is the reason for the observed increase in oxygen mobility (Figure 9).

This paper discusses a perovskite as a proper pathway for the rapid transport of oxygen in highly defective (mayenite-like) garnet. Indeed, lanthanum ferrites exhibit high (up to 10^{-5} S · cm^{-1}) oxygen mobility at 800 °C if they are doped with appreciable amounts of strontium to create oxygen vacancies [42]. The activation energy of oxygen transfer in these lanthanum ferrites is of about 0.8 eV, which is dramatically different from the data in Figure 7.

4. Conclusions

Pore-free $(Y_{0.82}La_{0.18})_3Fe_5O_{12}$ samples were grown by the floating zone method in various atmospheres using previously synthesized precursors with confirmed homogeneity of composition. The content of oxygen during the growth process determines its crystal structure: only in an oxygen atmosphere (7 atm) is it possible to obtain a single-phase crystal. The phase decomposes with precipitation of iron oxide when the oxygen content is lower.

Despite the fact that X-ray diffraction proved that samples are single crystals, fibers of submicron thickness along the direction of crystal growth are observed by an electron microscope. According to the cations ratio, these inclusions have a perovskite structure.

The samples demonstrate the predominant electrical nature of the total conductivity. The oxygen mobility in the studied samples is significantly higher than in conventional garnets, which is confirmed by the oxygen isotope exchange method.

Supplementary materials

This manuscript contains supplementary materials, which are available on a corresponding online page.

Funding

This work was supported by the project "Fundamental research of materials for solid oxide electrochemical devices" (122020100209-3). Part of the work devoted to the growth of single crystals and was partially supported by state assignment of Ministry of Science and Higher Education of the Russian Federation (theme "Spin" No. 122021000036-3).

Acknowledgments

The materials attestation was carried out in the Shared Access Centers of IHTE UB RAS and M.N. Mikheev Institute of Metal Physics UB RAS. Authors thank Dr. N.M. Porotnikova and A.V. Khodimchuk for technical support and useful comments on the manuscript of this paper.

Author contributions

Sergey Shkerin: Conceptualization; Methodology; Resources; Investigation; Writing – Original draft.

Anna Tolkacheva: Resources; Investigation; Writing – Review & Editing.

Sergey Naumov: Investigation; Resources.

Olga Gyrdasova: Investigation; Resources; Writing – Review & Editing.

Anton Stepanov: Investigation; Resources.

Conflict of interest

There are no conflicts to declare.

Additional information

Sergey Shkerin, Orcid: 0000-0003-4064-0670; Author ID: 55996378200;

Anna Tolkacheva, Orcid: 0000-0002-7546-7807; Author ID: 43462214600;

Sergey Naumov, Orcid: 0000-0003-4527-6396; Author ID: 57087543200;

Olga Gyrdasova, Orcid: 0000-0002-0680-6094; Author ID: 6602376811.

References

1. Heraeus WC. Uber die elektrolytische Leitung Fester Korper bei sehr hohen. Temperaturen, Elektrochem., 6(2) (1899) 41–43. https://doi.org/10.1002/bbpc.18990060205

2. Ishihara T, Matsuda H, Takita Y, Doped $LaGaO_3$ Perovskite Type Oxide as a New Oxide Ionic Conductor, J. Am. Ceram. Soc., **116** (1994) 3801–3803. https://doi.org/10.1021/ja00088a016

3. Feng M, Goodenough JB, A superior oxide-ion electrolyte, European Journal of Solid State and Inorganic Chemistry, **31** (1994) 663–672. https://doi.org/10.1002/CHIN.199507014

4. Liu H, Yuan L, Wang S, Fang H, et al., Structure, optical spectroscopy properties and thermochromism of $Sm_3Fe_5O_{12}$ garnets, J. Mater. Chem. C, **4** (2016) 10529–10537. https://doi.org/10.1039/c6tc02830f

5. Yamagishi T, Awaka J, Kawashima Y, Uemura M, et al., Ferrimagnetic order in the mixed garnet $(Y_{1-x}Gd_x)_3Fe_5O_{12}$, Philos. Mag., **85(17)** (2005–2006), 1819–1833. https://doi.org/10.1080/09500830500038092

6. Phan MH, Morales MB, Chinnasamy CN, Latha B, et al., Magnetocaloric effect in bulk and nanostructured $Gd_3Fe_5O_{12}$ materials, J. Phys. D: Appl. Phys., **42** (2009) 115007. https://doi.org/10.1088/0022-3727/42/11/115007

7. Al-Omari IA, Skomski R, Sellmyer DJ, Magnetic Properties of $Y_{3-2x}Ca_{2x}Fe_{5-x}V_xO_{12}$ Garnets, AMPC, **2** (2012) 116–120. https://doi.org/10.4236/ampc.2012.23019

8. Jiang L, Yang Sh, Zheng M, Chen H, Wu A, Synthesis and magnetic properties of nanocrystalline $Gd_3Fe_5O_{12}$ and $GdFeO_3$ powders prepared by sol–gel auto-combustion method, Mater. Res. Bull., **104** (2018) 92–96. https://doi.org/10.1016/j.materresbull.2018.04.010

9. Cherepanov V, Kolokolov I, L'vov V, The saga of YIG: Spectra, thermodynamics, interaction and relaxation of magnons in a complex magnet, Phys. Rep., **229(3)** (1993) 81–144. https://doi.org/10.1016/0370-1573(93)90107-O

10. Gomez-Perez JM, Oyanagi K, Yahiro R, Ramos R, Absence of evidence of spin transport through amorphous $Y_3Fe_5O_{12}$, Appl. Phys. Lett., **116(3)** (2020) 032401. https://doi.org/10.1063/1.5119911

11. Fechine PBA, Moretzsohn RST, Costa RCS, Derov J, et al., Magneto-dielectric properties of the $Y_3Fe_5O_{12}$ and gd3fe5o12 dielectric ferrite resonator antennas, ASB Microw. Opt., **50(11)** (2008) 2852–2857. https://doi.org/10.1002/mop.23824

12. Guo X, Rak Zs, Tavakoli AH, Becker U, et al., Thermodynamics of thorium substitution in yttrium iron garnet: comparison of experimental and theoretical results, J. Mater. Chem. A, **2** (2014) 16945–16954. https://doi.org/10.1039/c4ta03683b

13. Guo X, Rak Zs, Tavakoli AH, Sutton S, et al., Cerium Substitution in Yttrium Iron Garnet: Valence State, Structure, and Energetics, Chem. Mater., **26(2)** (2014) 1133–1143. https://doi.org/10.1021/cm403444f

14. Guo X, Kukkadapu RK, Lanzirotti A, Newville M, et al., Charge-Coupled Substituted Garnets $(Y_{3-x}Ca_{0.5x}M_{0.5x})Fe_5O_{12}$ (M = Ce, Th): Structure and Stability as Crystalline Nuclear Waste

Forms, Inorg. Chem., **54(8)** (2015) 4156–4166. https://doi.org/10.1021/acs.inorgchem.5b00444

15. Guo X, Navrotsky A, Kukkadapu RK, Engelhard MH, et al., Structure and thermodynamics of uranium-containing iron garnets, Geochimica et Cosmochimica Acta, **189** (2016) 269–281. https://doi.org/10.1016/j.gca.2016.05.043

16. Long GJ, Grandjean F, Guo X, Navrotsky A, et al., Mossbauer Spectral Properties of Yttrium Iron Garnet, $Y_3Fe_5O_{12}$, and Its Isovalent and Nonisovalent Yttrium-Substituted Solid Solutions, Inorg. Chem., **55(7)** (2016) 3413–3418. https://doi.org/10.1021/acs.inorgchem.5b02769

17. Navrotsky A, Lee W, Mielewczyk-Gryn A, Ushakov SV, et al., Thermodynamics of Solid Phases Containing Rare Earth Oxides, J. Chem. Thermodyn., **88** (2015) 126–141. https://doi.org/10.1016/j.jct.2015.04.008

18. Becker S, Ren Z, Fuhrmann F, Ross A, et al., Magnetic Coupling in $Y_3Fe_5O_{12}/Gd_3Fe_5O_{12}$ Heterostructures, Phys. Rev. Applied, **16** (2021) 014047. https://doi.org/10.1103/PhysRevApplied.16.014047

19. Mullerbuschbaum H, Vonpostel M, Eine weitere Oxovanadat-Phase mit Granatstruktur: $Ca_5Mg_3ZnV_6O_2$, Allg. Chem., **615(9)** (1992) 101–103. https://doi.org/10.1002/zaac.19926150920

20. Baettig P, Oguchi T, Why Are Garnets Not Ferroelectric? A Theoretical Investigation of $Y_3Fe_5O_{12}$, Chem. Mater., **20** (2008) 7545–7550 https://doi.org/10.1021/cm801786h

21. Shkerin SN, Tolkacheva AS, Mayenite (A Review), Russian Journal of General Chemistry, **92(11)** (2022) 2312–2333. https://doi.org/10.1134/S1070363222110160

22. Larsen PK, Metselaar R, Defects and the Electronic Properties of $Y_3Fe_5O_{12}$, J. Solid State Chem., **12(3–4)** (1975) 254–258. https://doi.org/10.1016/0022-4596(75)90315-1

23. KJacob KT, Rajitha G, Nonstoichiometry, defects and thermodynamic properties of $YFeO_3$, YFe_2O_4 and $Y_3Fe_5O_{12}$, Solid State Ion., **224** (2012) 32–40 https://doi.org/10.1016/j.ssi.2012.07.003

24. Huang S, Shi LR, Sun HG, Li CL, et al., High temperature dielectric response in $Sm_3Fe_5O_{12}$ ceramics, J. Alloys Compd., **674** (2016) 341–346. https://doi.org/10.1016/j.jallcom.2016.03.001

25. Kharton VV, Shaula AL, Naumovich EN, Vyshatko NP, et al., Ionic Transport in $Gd_3Fe_5O_{12}$- and $Y_3Fe_5O_{12}$-Based Garnets, J. Electrochem. Soc., **150(7)** (2003) J33–J42. https://doi.org/10.1149/1.1574810

26. Waerenborgh JC, Rojas DP, Shaula AL, Kharton VV, et al., Defect formation in $Gd_3Fe_5O_{12}$-based garnets: a Mfssbauer spectroscopy study, Mater Lett., **58** (2004) 3432–3436. https://doi.org/10.1016/j.matlet.2004.05.081

27. Paladino AE, Maguire EA, Rubin LG, Oxygen Ion Diffusion in Single-Crystal and Polycrystalline Yttrium Iron Garnet, J. Am. Ceram. Soc., **47(6)** (1964) 280–282. https://doi.org/10.1111/j.1151-2916.1964.tb14416.x

28. Kilner JA, Steele BCH, Ilkov L, Oxygen self-diffusion studies using negative-ion secondary ion mass spectrometry (SIMS), Solid State Ion., **12** (1984) 89–97. https://doi.org/10.1016/0167-2738(84)90134-6

29. Shkerin SN, Ulyanova ES, Naumov SV, Shmakov AN, et al., The interaction of defects in a mayenite structure, Phys. Chem. Chem. Phys., **22** (2020) 27818–27828. https://doi.org/10.1039/d0cp05107a

30. Tolkacheva AS, Shkerin SN, Porotnikova NM, Kuznetsov MV, et al., Oxygen surface exchange and diffusion in mayenite single crystal, Phys. Chem. Chem. Phys., **21** (2019) 24740–24748. https://doi.org/10.1039/C9CP04936C

31. Bhosale DR, Yusuf SM, Kumar A, Mukadam MD, et al., High oxide ion conductivity below 500 °C in the garnets $La_xY_{3-x}Fe_5O_{12+\delta}$, Phys. Rev. Mater., **1** (2017) 015001. https://doi.org/10.1103/PhysRevMaterials.1.015001

32. Yousaf M, Akhtar MN, Yousaf Shah MAK, Rauf S, et al., Evaluation of rare earth (Yb, La) doped ($Sm_3Fe_5O_{12}$) garnet ferrite membrane for LT-SOFC, Int. J. Hydrogen Energy., **46** (2021) 9996–10006. https://doi.org/10.1016/j.ijhydene.2020.01.166

33. Gyrdasova OI, Stepanov AE, Naumov SV, Shkerin SN, The influence of synthesis conditions on the formation of the $Y_{3-x}La_xFe_{5-y}O_{12+\delta}/La_{1-x}Y_xFe_{1-y}O_3$ composite, Physical and chemical aspects of the study of clusters, nanostructures and nanomaterials, **14** (2022) 583–592. (In Russian). https://doi.org/10.26456/pcascnn/2022.14.583

34. Gyrdasova OI, Pasechnik LA, Krasilnikov VN, Surikov VT, Kuznetsov MV, Sorption and photocatalytic activity of $Zn_{1-x}Cu_xO$ (x = 0.05 and 0.15) to As(III) in alkaline medium, Physical and chemical aspects of the study of clusters, nanostructures and nanomaterials, **12** (2020) 792–804. (In Russian). https://doi.org/10.26456/pcascnn/2020.12.792

35. Ezin AN, Tsidilkovski VI, Kurumchin EKh, Isotopic exchange and diffusion of oxygen in oxides with different bulk and subsurface diffusivities, Solid State Ion., **84(1–2)** (1996) 105–112. https://doi.org/10.1016/S0167-2738(96)83012-8

36. Klier K, Kučera E, Theory of exchange reactions between fluids and solids with tracer diffusion in the solid, J. Phys. Chem. Solids, **27(6–7)** (1966) 1087–1095. https://doi.org/10.1016/0022-3697(66)90084-9

37. Mizusaki J, Mima Y, Yamauchi S, Fueki K, et al., Nonstoichiometry of the perovskite-type oxides $La_{1-x}Sr_xCoO_{3-\delta}$, Solid State Chem., **80(1)** (1989) 102–111. https://doi.org/10.1016/0022-4596(89)90036-4

38. Ananyev MV, Tropin ES, Eremin VA, Farlenkov AS, et al., Oxygen isotope exchange in $La_2NiO_{4\pm d}$, Phys. Chem. Chem Phys., **18** (2016) 9102–9111. https://doi.org/10.1039/C5CP05984D

39. Lyubutin IS, Gavriliuk AG, Trojan IA, Sadykov RA, Magnetic Collapse in Yttrium Iron Garnet $Y_3Fe_5O_{12}$ at High Pressure, Jetp. Lett., **82** (2005) 702–707. https://doi.org/10.1134/1.2171723

40. Rotman S, Tuller H, Defect-Property Correlations in Garnet Crystals. *VII: The Electrical Conductivity and Defect Structure of Yttrium Aluminum and Yttrium Iron Garnet Solid Solutions, J. Electroceram., **2** (1998) 95–104. https://doi.org/10.1023/A:1009974923893

41. Yaremchenko AA, Kharton VV, Viskup AP, Naumovich EN, et al., Oxygen Ionic and Electronic Transport in $LaGa_{12x}Ni_xO_{32d}$ Perovskites, J. Solid State Chem., **142(2)** (1999) 325–335. https://doi.org/10.1006/jssc.1998.8041

42. Elshof JE, Lankhorst MHR, Bouwmeester HJM, Oxygen Exchange and Diffusion Coefficients of Strontium-Doped Lanthanum Ferrites by Electrical Conductivily Relaxation, J. Electrochem Soc., **144(3)** (1997) 1060–1066. https://doi.org/10.1149/1.1837531